Retrieval of the Seismic Moment Tensor from Joint Measurements of Translational and Rotational Ground Motions: Sparse Networks and Single Stations

Stefanie Donner, Heiner Igel, Céline Hadziioannou and the Romy group

Abstract Seismic moment tensors help us to increase our understanding about e.g. earthquake processes, tectonics, Earth or planetary structure. Based on ground motion measurements of seismic networks their determination is in general standard for all distance ranges, provided the velocity model of the target region is known well enough. For sparse networks in inaccessible terrain and planetary seismology, the waveform inversion for the moment tensor often fails. Rotational ground motions are on the verge of becoming routinely observable with the potential of providing additional constraints for seismic inverse problems. In this study, we test their benefit for the waveform inversion for seismic moment tensors under the condition of sparse networks. We compare the results of (1) inverting only traditional translational data with (2) inverting translational plus rotational data for the cases of only one, two, and three stations. Even for the single station case the inversion results can be improved when including rotational ground motions. However, from data of a single station only, the probability of determining the correct full seismic moment tensor is still low. When using data of two or three stations, the information gain due to rotational ground motions almost doubles. The probability of deriving the correct full moment tensor here is very high.

S. Donner (✉)
Bundesanstalt für Geowissenschaften und Rohstoffe (BGR), Hannover, Germany
e-mail: stefanie.donner@lmu.de; stefanie.donner@bgr.de
URL: http://romy-erc.eu

S. Donner · H. Igel · the Romy group
Ludwig-Maximilians-University Munich, Munich, Germany

C. Hadziioannou
University of Hamburg, Hamburg, Germany

S. D'Amico (ed.), *Moment Tensor Solutions*, Springer Natural Hazards,
https://doi.org/10.1007/978-3-319-77359-9_12

1 Introduction

1.1 Why Single Station/Sparse Network?

Regional and local seismic moment tensors are an important observation for various applications, such as spatio-temporal analysis of earthquake sequences, volcanic studies, monitoring of geothermal facilities, and tomographic studies. In order to avoid errors, the moment tensors must be determined precisely. However, this objective can be challenging, especially in the regional/local distance range, where waveforms are more complex than in the teleseismic distance range.

Usually, translational ground motion observations from a network of stations are used to determine the seismic moment tensor. The more data are available and the better the stations are distributed around the source in distance and azimuth (thus sampling the entire radiation pattern), the better is the resolution of the determined moment tensor. However, in inaccessible environments such as deserts or arctic regions it is not always possible to install a large network. Even worse, in planetary seismology often only single observation sites can be instrumented (e.g. InSight: Banerdt et al. 2013). The examination and understanding of the structure of other planets such as Mars and Moon are hampered because most seismological methods are based on station networks. Establishing entire networks on other planets is logistically and economically impossible, at least for now. Therefore, the question remains if and to what extent the full seismic moment tensor is resolvable from data of just one single station or a sparse network of maximum three stations.

1.2 Difficulties in the Single Station Approach

Theoretically, the three components of translational motion recorded at a single location should be sufficient to unambiguously determine the full seismic moment tensor in the teleseismic distance range (Ekström et al. 1986). Converted into an event-centric coordinate system (ZRT) the different wave types P, SV, and SH can be separated on the three components. Their amplitude ratios then provide the necessary information about the mechanism. However, in the regional distance range waveforms are more complex and more strongly influenced by noise. In addition, the inversion is performed on surface waves rather than on body waves. Especially for shallow sources this approach results in difficulties for the resolution of specific moment tensor components (e.g. Bukchin 2006; Bukchin et al. 2010). Therefore, the single station approach almost always fails in the regional distance range.

1.3 Rotational Ground Motions and Outline

Rotational ground motions are a relatively new observable, providing an additional three out of twelve components that completely describe the motion of a measurement

point. So far, this observable has often been ignored, since compared to the traditional three components of translation it is much smaller (up to a factor 10^{-9}) and suitable measurement devices were not available. Only recently, sensitive portable broadband measurement devices based on fibre-optic techniques are available (Bernauer et al. 2018).

Rotation $\vec{\omega}$ is the curl of the wave field defined through a linear combination of the space derivatives of the translation vector $\vec{u}$:

$$\begin{pmatrix} \omega_x \\ \omega_y \\ \omega_z \end{pmatrix} = \frac{1}{2} \begin{pmatrix} \partial_x \\ \partial_y \\ \partial_z \end{pmatrix} \times \begin{pmatrix} u_x \\ u_y \\ u_z \end{pmatrix} = \frac{1}{2} \begin{pmatrix} \partial_y u_z - \partial_z u_y \\ \partial_z u_x - \partial_x u_z \\ \partial_x u_y - \partial_y u_x \end{pmatrix} \tag{1}$$

where $\times$ denotes a vector product. Measured at the Earth's surface, the horizontal components of rotation are commonly known as tilt. Rotational ground motions provide us with information about the vertical displacement gradient which is not available from conventional seismic stations on the Earth's surface.

In an earlier study, we could numerically show that data of a network based on six component measurement devices (3 translations + 3 rotations) considerably improves the resolution of the full moment tensor when performing a Bayesian (i.e. probabilistic) waveform inversion while keeping the total number of components constant (Donner et al. 2016). Motivated by the promising results of this earlier study, here, we evaluate the benefits of rotational ground motions for single or sparse station configurations.

In addition to the Bayesian inversion using the set-up of the former study, we also show the analytical solution for a double-couple moment tensor in a homogeneous space for translational and rotational ground motion. We will use the analytical solution to discuss under which geometries the reliable retrieval of the seismic moment tensor has the highest probability.

2 The Test Case Scenario and Applied Method

In an earlier study, we designed a synthetic earthquake scenario in Iran to analyse the performance of an entire network for waveform inversion to retrieve seismic moment tensors (Donner et al. 2016). The motivation was to examine the benefits of rotational ground motion measurements for the moment tensor retrieval. For this purpose, we have calculated Greens functions for two scenarios: one based on the real station distribution of the Iranian broadband network and one based on a fictional grid of stations covering the whole country. In this study, we continue with the fictive grid of stations and evaluate the cases when only one, two, or three stations are available. In the following, we briefly review the set-up of the experiment and the Bayesian, i.e. probabilistic, inversion approach.

2.1 Set-Up of the Synthetic Test Case

In Fig. 1 the blue star marks the location of the synthetic earthquake in north-central Iran. It is an almost vertical strike-slip event with a magnitude M_w4.0 at a depth of 6 km. Its double-couple (DC) and isotropic (ISO) parts have 80% and 15%, respectively. The full moment tensor is given by

$$M_{kj} = \begin{pmatrix} -0.75 & -0.16 & 0.41 \\ & 1.17 & 0.26 \\ & & 0.02 \end{pmatrix} \tag{2}$$

The theoretically observed waveforms as well as the Greens functions are calculated using a spectral-element solver based on a 1-D structural model for the Alborz mountains (Fichtner et al. 2009; Donner et al. 2013). Gaussian noise was added to the synthetic seismograms to render them more realistic. For this study, since only the relative noise levels are relevant, we applied a noise of 10% of the maximum amplitude and evaluate translation and rotation data separately.

The fictional stations are distributed equally covering almost the whole surface of Iran (Fig. 1). There is a grid of 21 by 31 stations along latitude and longitude, respectively. The Greens functions are calculated for depths between 2 and 20 km in 2 km steps for frequencies up to 0.1 Hz to include surface waves, which are usually used for inversion in the regional distance range.

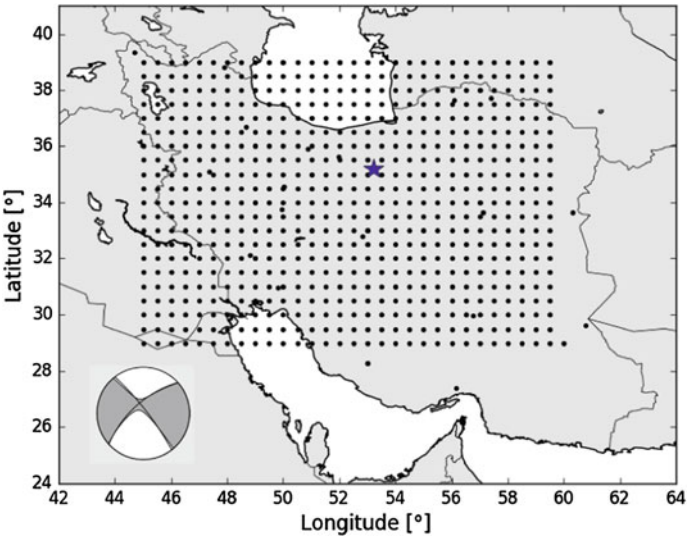

Fig. 1 Study area in Iran. The blue star marks the position of the synthetic M_w4.0 earthquake. The mechanism is shown in the lower left with black lines and grey shaded areas being the nodal planes of the double-couple part and the full moment tensor solution, respectively. Black dots show the grid of theoretical stations

2.2 Probabilistic Waveform Inversion for Seismic Moment Tensors

Probabilistic, i.e. Bayesian, inversion has the advantage that it results in a solution class instead of one single solution. A selection of "the best" solution according to a more or less subjective criterion is omitted. Thus, Bayesian inversion provides an unbiased measure of resolution and possible trade-offs.

As in our former studies, we use the Bayesian inversion approach based on equations from Tarantola (2005):

$$\sigma(\mathbf{m}) = k\rho(\mathbf{m})L(\mathbf{m}) \tag{3}$$

where $\sigma(\mathbf{m})$ and $\rho(\mathbf{m})$ are the *posterior* and *prior probability density functions* (pdf) of the model parameters, respectively, k is a normalization constant, and $L(\mathbf{m})$ is the likelihood function providing a measure of how well a model $\mathbf{m}$ fits the data.

The inversion is performed for seven parameters, i.e. the six moment tensor components and centroid depth, in the time domain according the forward problem for the seismic point-source moment tensor (Aki and Richards 2002):

$$u_n(\mathbf{x}, t) = M_{kj} \cdot G_{nk,j}(\mathbf{x}, t - \tau) \tag{4}$$

with u_n is the ground motion at observation point $\mathbf{x}$ and time t, M_{kj} the components of the seismic moment tensor, and $G_{nk,j}$ the spatial derivatives of the Green's function components. τ is the origin time of the source. Einstein summation convention was applied to facilitate readability of the equation.

The *posterior pdf* is approximated from the homogeneous *prior pdf* by testing one million start models by applying the Metropolis-Hastings algorithm (e.g. Metropolis et al. 1953; Hastings 1970). Intuitively spoken, this algorithm performs a random walk through the model space. Based on Eq. 4 waveforms for the model candidate are calculated and compared to the theoretical observations. Depending on whether or not the model candidate improves the data fit, it will be added to the solution class or not.

For an objective estimate on the information content of the *posterior* relative to the *prior pdf* we use Shannon's measure of information gain:

$$I(\rho, \sigma) = \int \rho(x) \log \left[\frac{\rho(x)}{\sigma(x)} \right] dx. \tag{5}$$

Due to the logarithm base 2 in Eq. 5, the unit of the information gain is termed a *bit*. For further details on the set-up, on the method and Shannon's measure of information gain, we refer to our earlier studies (Bernauer et al. 2014; Donner et al. 2016; Reinwald et al. 2016) and to (Tarantola 2005).

3 Results

In the following, we show the results of the inversion of the theoretically observed waveforms for the test case shown in Fig. 1 and described in Sect. 2. We tested three scenarios with only one, two and three stations. For each scenario, we performed 670 inversions where we first inverted only translational ground motions and then repeated the 670 inversions inverting translational and rotational ground motions. For each inversion, the station(s) are randomly selected from the grid of possible stations. For each scenario, we show the generalised result over all 670 inversions along with the result of the inversion with the best outcome.

3.1 Single Station

Figure 2 shows the generalised result of the 670 inversions based on data of only one station. Each sub-plot represents one of the seven parameters inverted for. The x-axes show the value of Shannon's measure of information gain, while the y-axes show the Gaussian kernel density estimations (kde), i.e. the marginal probability density function over the information gain. The higher the information gain, the better is the resolution of the parameters inverted for. Coral and green functions give the results for inversion of translational data only and translational with rotational data, respectively. The same colour-coding is used for all following figures.

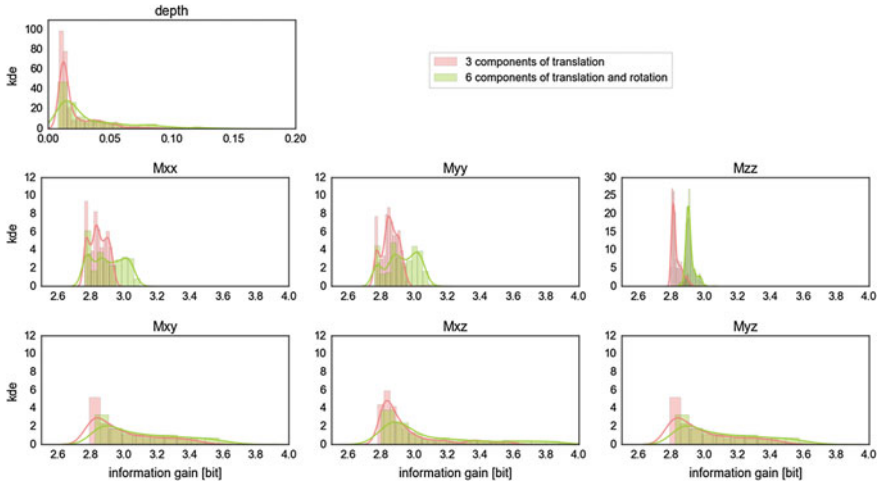

Fig. 2 Gaussian kernel density estimations (kde) for the information gain corresponding to 670 inversions for the **single station case**. Coral and green distributions show the results for inverting translational ground motions only and translational with rotational ground motions, respectively. The higher the information gain, the better is the resolution of the parameters

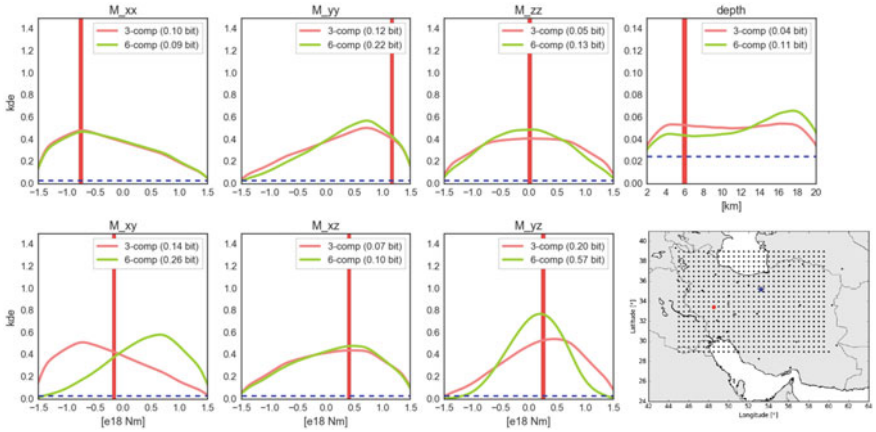

Fig. 3 Inversion result for the **single station case** for the inversion with highest information gain (0.72/1.48 bit for 3/6 components). The station used for this inversion is marked by a red dot on the map. The red bars show the real value of the target solution. Blue dotted lines are the homogeneous *prior pdf*. Coral and green curves show the *posterior pdf* for inversion of translations only and translations plus rotations, respectively. Numbers in the upper right corner give increase of information content relative to the prior according to Shannon's measure

No matter which of the stations within the grid is used, four out of the seven parameters almost never benefit from the inclusion of rotational ground motions. These are the centroid depth and the moment tensor components M_{xy}, M_{xz}, and M_{yz}. In contrast, the other three components M_{xx}, M_{yy}, and M_{zz} can benefit remarkably. Especially the component M_{zz} almost always benefits from the inclusion of rotational ground motions, no matter which station is used for the inversion.

The question remains whether the real moment tensor solution was determined. Figure 3 shows the result of only one of the 670 inversions, the one with the highest resulting information gain. For each of the parameters inverted for the *posterior pdf* kde's are plotted over the parameter space. In the upper right corners the information gains are given. The vertical red bars show the real values of the target solution. Most of the parameters benefit only slightly from the rotational ground motions, except for the moment tensor component M_{yz} which shows a substantial improvement. For the components M_{yy}, M_{xy}, and the centroid depth the highest probability is not at the real value of the target model. When considering the rotational ground motions, the highest probability for centroid depth is different from the true value. Despite this, the overall benefit of the rotational ground motion for inversion based on a single station, i.e. the increase in information gain, is 105% (Fig. 3, $(1.48 - 0.72) * 100/0.72$).

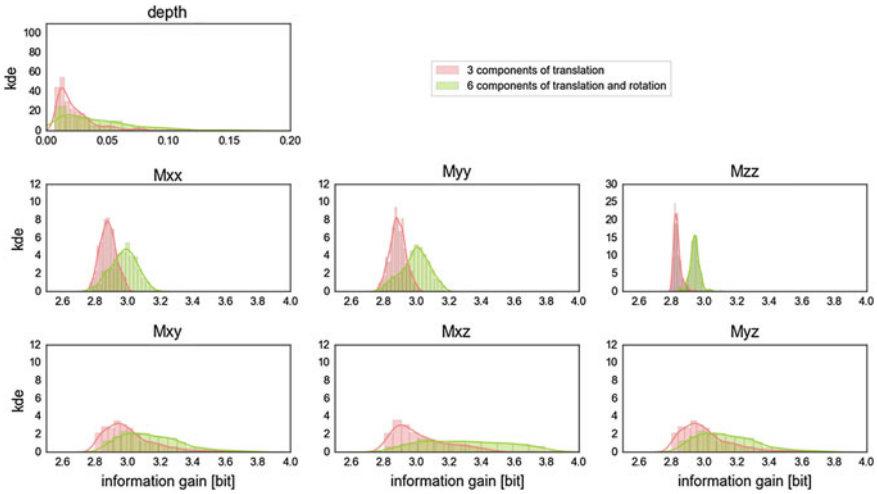

Fig. 4 Generalized inversion results for the **two station case**. Colour-coding is the same as in Fig. 2

3.2 Two Stations

Figure 4 shows the generalised result of the 670 inversions based on data from two stations. Now, compared to the single station case, the green kde functions (6-component data) of the components M_{xy}, M_{xz}, and M_{yz} are slightly shifted to higher values for information gain compared to the coral kde functions. These shifts indicate that these components have a higher probability to be determined reliably when including rotational ground motions to the inversion based on two stations. In addition, the probability to estimate the correct centroid depth is increased. For the remaining three moment tensor components the benefits due to rotations are also more pronounced.

The result of the inversion with the highest resulting information gain (0.98/2.73 bit for 3/6 components) based on data from two stations is shown in Fig. 5. Almost all moment tensor components show a much higher probability to be determined correctly when including rotational ground motions, except the component M_{xy}. By far the biggest improvement can be seen for the moment tensor component M_{xz}. The most critical parameter is still the centroid depth, which again shows a low probability to be resolved. The overall increase in information gain is 178%, almost 75% more than for the single station case.

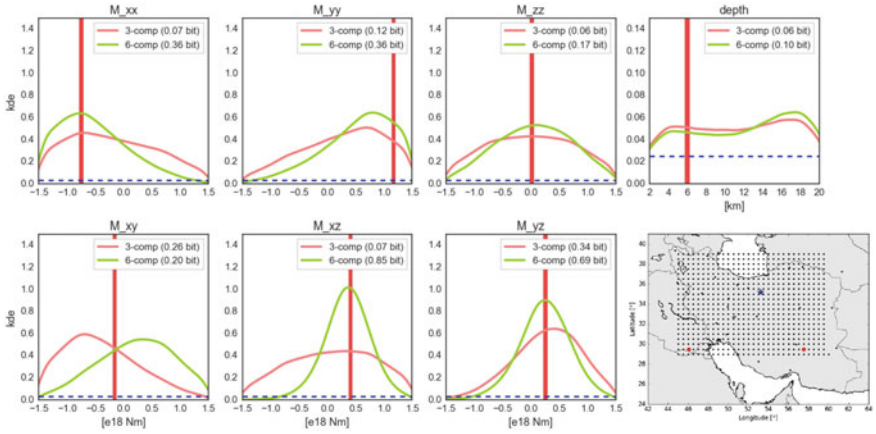

Fig. 5 Inversion result for the **two station case** for the inversion with highest information gain (0.98/2.73 bit for 3/6 components). The stations used for this inversion are marked by red dots on the map. Colour-coding is the same as in Fig. 3

3.3 Three Stations

Figure 6 shows the generalised result of the 670 inversions based on data from three stations. As expected, the shift to values of higher information gain of the green kde's (6-component data) compared to the coral kde's (3-component data) is much more

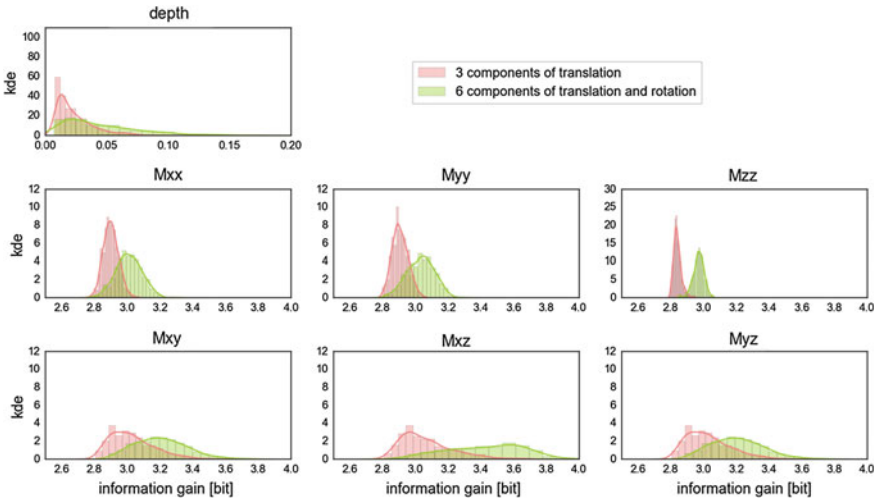

Fig. 6 Generalized inversion results for the **three station case**. Colour-coding is the same as in Figs. 2 and 4

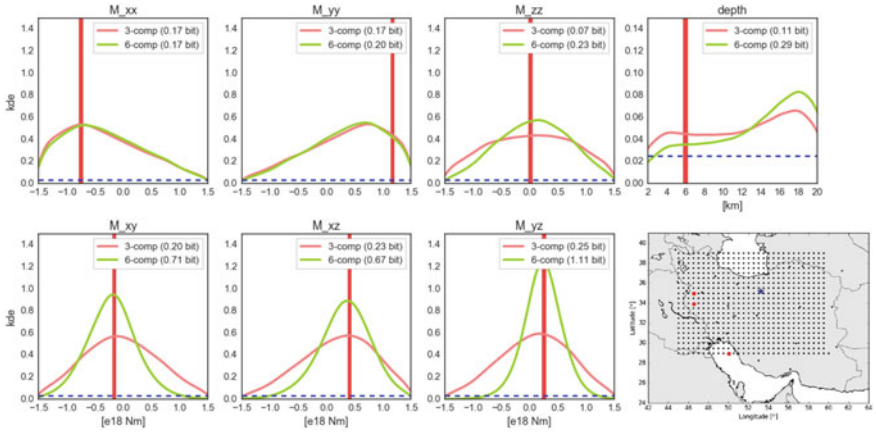

Fig. 7 Inversion result for the **three station case** for the inversion with highest information gain (1.20/3.38 bit for 3/6 components). The stations used for this inversion are marked by red dots on the map. Colour-coding is the same as in Figs. 3 and 5

distinct for all moment tensor components compared to the two station case. The overlap between coral and green curves is greatly reduced, implying that for almost all station distributions, the inclusion of the rotational ground motion data results in a much higher probability of producing in the correct solution.

The result of only one inversion showing the best result (i.e. highest information gain) based on three stations is shown in Fig. 7. Now, there is even a significant probability to retrieve the correct moment tensor from translational data alone (coral functions). However, the probability is 181% higher when including the rotational ground motions. Especially the components including depth dependencies (M_{xz}, M_{yz}, and M_{zz}) and the component M_{xy} benefit most from including rotational data into the inversion. The probability of retrieving the correct centroid depth is still low.

4 Discussion and Conclusion

In this study, we evaluated the retrieval of seismic moment tensors under the assumption of having data from only one, two, or three stations with both translational and rotational ground motions. The study is based on a theoretical scenario in Iran already used in an earlier study, where we evaluated the performance of a network under consideration of rotational ground motions (Donner et al. 2016). For each station case, we have performed a Bayesian, i.e. probabilistic, inversion once only using translational and once using translational plus rotational ground motions. We have repeated these inversions 670 times, always randomly selecting station(s) out of a grid of theoretical station locations (Fig. 1). Next to the generalized results based on these

670 inversions (Figs. 2, 4 and 6), we also showed the results of the inversion with the highest information gain (Figs. 3, 5 and 7).

The results show that it might be difficult to fully retrieve the moment tensor from one station alone. Figure 3 shows that even when including the rotations, the probability to retrieve the true values for the inversion parameters is not very high. Nevertheless, the increase of information gain due to the rotations is still 105%. Here, we tested the inversion for the full moment tensor. There might be a chance to retrieve at least the mechanism of an earthquake from data of a single station when applying constraints to the inversion. Finally, when including data of a second and third station the probability to retrieve the correct full moment tensor is very high. The overall increase of information gain is 178% for two and 181% for three 6-component stations. The generalisations of the two and three station case in the Figs. 4 and 6 show that this is the case for a wide range of station distributions. Especially for planetary seismology, this is an important result. It might be logistically and economically possible to bring two or three instruments to another planet such as Mars or Moon, even though the locations for these instruments would be determined according to practical rather than scientific criteria.

Centroid depth is the only parameter which in all station cases has a very low probability of being resolved. This effect is a general problem in waveform inversion for moment tensors. Especially, in the regional distance range, where inversion is done on surface waves, and for shallow earthquakes depth is a very critical parameter (e.g. Bukchin 2006; Bukchin et al. 2010). Our test case scenario includes exactly these difficulties. Therefore, the unsatisfying results for centroid depths are to be expected.

The question remains what the cause for the benefit from rotational data is. As can be seen from Eq. 1, rotational ground motions are linear combinations of the space derivatives of the translational ground motions. Measured at the Earth surface, their horizontal components correspond to tilt. Therefore, rotational ground motions include information about the velocity gradient with depth which is not available from translational ground motions. However, the comparison is not completely fair. When including the rotational ground motions, we have doubled the number of data (3 versus 6 traces for the single station case). Thus, the improved inversion results may be partly due to higher amount of information. However, in our former study based on an entire network, we kept the number of data in both cases the same (by cutting the number of stations in half when including rotational ground motions) and still received greatly improved inversion results. Therefore we argue that the increased amount of data is responsible only for a small portion of the improvement, if at all.

Already in 1986, when waveform inversion for moment tensors was newly established as a standard in the teleseismic distance range, Ekström et al. successfully inverted waveforms of the 1985 M 8.1 Michoacan, Mexico, earthquake from only three components of translational data for the deviatoric moment tensor (i.e. isotropical part is constrained; $ISO = \mathrm{tr}\, M_{ij} = 0$). They emphasised the necessity of a very good signal-to-noise ratio (SNR), a recording system with a broad frequency response and large dynamic range (not standard at that time), a well known velocity model, and exclusion of antipodal event-station geometry. Nowadays, three out of

these four criteria are fulfilled in the teleseismic distance range and strong enough earthquakes result in a good SNR. Due to the well developed global seismic network it is now also possible to find an appropriate station, which meets the geometry criterion. However, in the regional distance range this approach is hampered due to more complex waveforms, less well known velocity models, and a limited number of stations. Jiménez et al. (1989) have extended the approach of Ekström et al. (1986) to regional and moderate-sized (i.e. $M_S \approx 4.5 - 5.5$) earthquakes. They further limited the inversion to the double-couple part of the moment tensor (i.e. tectonic part; $DC = \det M_{ij}^{dev} = 0$) and emphasized the need for path corrections using the dispersion properties of Love and Rayleigh waves. Fan and Wallace (1991) used a similar approach and found a trade-off between structure and depth in that a reliable mechanism might come with a "wrong" depth due to inaccuracies in the assumed structural model. Additionally, they stated that the noise level should be 10% as a maximum to retrieve a reliable mechanism. The results of these studies based on only three components of translation combined with the results of the Bayesian inversion in this study are promising. We are confident that having six components available there are chances to at least determine the deviatoric moment tensor reliably from a single station measurement, if not the full moment tensor.

The velocity model needed to calculate the Greens functions used for inversion is the more crucial point in the entire process. In the regional distance range, a larger proportion of the seismic energy travels through the crust than in the teleseismic distance range (where the more homogeneous deeper structure of the Earth is more important). Thus, the structural details of the crust have a stronger influence on the waveforms and therefore cause the waveform complexities. In planetary seismology, where the structures are less well known than on Earth, the same difficulties will be faced. Sampling an additional part of the seismic wave field by including rotational ground motions into the inversion can compensate for these issues, at least partly.

Next to the velocity model, the event-station geometry is of great importance when restricted to only a few stations. In Fig. 8 we show the radiation pattern of the theoretical earthquake for the six components of translation and rotation. Each sub-plot shows the maximum energy for this specific earthquake mechanism and for each of the theoretical stations of the grid for the component mentioned above the sub-plot. Blue, green, and turquoise dots show the station(s) used for the best inversions for the single, two, and three station case shown in Figs. 3, 5, and 7. The energy is calculated as the square root of the sum of squared amplitudes divided by the maximum amplitude of the trace: $E = \sqrt{\sum tr_i^2}/A_{max}(tr)$.

When comparing the locations of the stations used within the radiation pattern of the different components, it is clearly visible that they lead to significant amplitude ratios between the different components. Inverting only waveforms of the three translational components results in only three amplitude ratios. The additional three components of rotation provide further three amplitude ratios of rotation plus further nine amplitude ratios of translation versus rotation. Therefore, the position within the radiation pattern at which the station(s) are located is better constrained. Not the single traces themselves but rather their amplitude ratios contribute to the

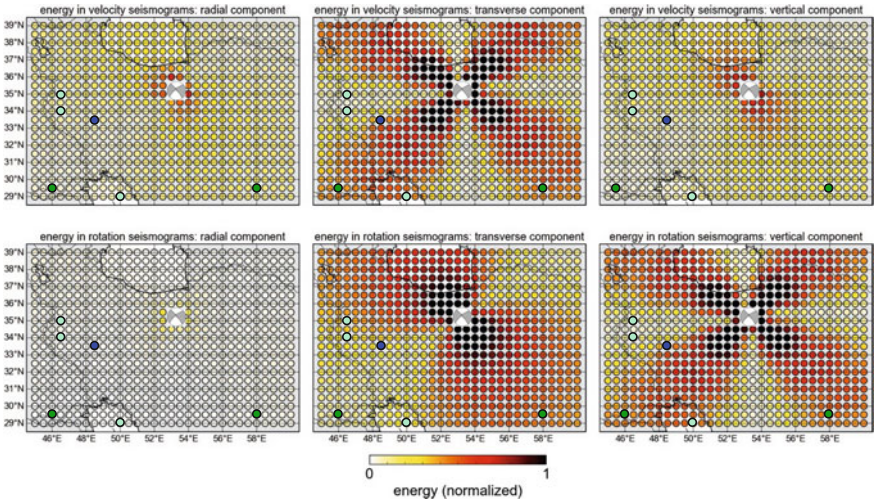

Fig. 8 Radiation pattern for the synthetic earthquake scenario in Iran (Fig. 1). The plots are in the event-centric cartesian coordinate system (ZRT). Top row shows radial, transverse, and vertical component of the velocity energy, respectively, while the bottom row shows the same for rotation. The mechanism of the theoretical earthquake is shown at its location. Blue, green, and turquoise dots show the station(s) used for the inversions based on one, two, and three stations, respectively; inversion results are shown in Figs. 3, 5 and 7

resolution of the moment tensor solution. Therefore, we think that it might be possible to at least derive the pure deviatoric mechanism from only one station, i.e. adding constraints to the waveform inversion. This argumentation is supported by the evaluation of the analytical solution for the radiation pattern of a double-couple source in a homogeneous medium in Appendix A.

In summary, there are two main crucial points when inverting waveforms for moment tensors from sparse networks: a limited knowledge of the underlying velocity model and the question where in the radiation pattern the station(s) is/are located. Including rotational ground motion data can at least partly compensate for these limitations. First, by sampling another property of the wave field, and second, by adding more input data, in the form of more components or local wavefield gradients. We see potential to greatly improve the performance of existing seismic networks with respect to waveform inversion for moment tensors by adding just one single rotational sensor to the network. In regions where the same mechanism occurs regularly, it is possible to find the most advantageous station position with respect to the radiation pattern.

Acknowledgements Parts of this study have been done using ObsPy (ObsPy Development Team 2015; Beyreuther et al. 2010; Megies et al 2011; Krischer et al. 2015) and we are very thankful to the developers. The research presented in this article was funded by the European Research Council (Advanced grant: ROMY, number: 339991). The numerical computations were performed

on the National Supercomputer SuperMUC maintained by the Leibniz-Rechenzentrum (Project ID: pr63qo).

Appendix: Analytical Solution for the Radiation Pattern of a Double-Couple Source

To further analyse the event station geometry with respect to the radiation pattern of a seismic source, in the following, we show the analytical solution of a double-couple source, i.e. the tectonic part of the seismic moment tensor.

The far-field displacement $u(\vec{x}, t)$ due to a double-couple point-source in an infinite, homogeneous, isotropic medium in a spherical coordinate system is (Aki and Richards 2002):

$$\mathbf{u}(\mathbf{x}, t) = \frac{1}{4\pi\rho\alpha^3}\mathbf{A}^{FP}\frac{1}{r}\dot{M}_0\left(t - \frac{r}{\alpha}\right) + \frac{1}{4\pi\rho\beta^3}\mathbf{A}^{FS}\frac{1}{r}\dot{M}_0\left(t - \frac{r}{\beta}\right) \tag{6}$$

where α, β, and ρ are the velocities for P- and S-wave and the density of the medium, respectively. r is the source-receiver distance and $M_0(t)$ the seismic moment function. A^{FP} and A^{FS} are the far-field radiation patters for the P- and S-wave in spherical coordinates:

$$\begin{aligned} \boldsymbol{A}^{FP} &= \sin 2\theta \cos\phi\hat{\boldsymbol{r}} \\ \boldsymbol{A}^{FS} &= \cos 2\theta \cos\phi\hat{\boldsymbol{\theta}} - \cos\theta \sin\phi\hat{\boldsymbol{\phi}} \end{aligned} \tag{7}$$

Similarly, the far-field rotation can be described as

$$\boldsymbol{\omega}(\mathbf{x},t) = \frac{-1}{8\pi\rho\beta^4}\boldsymbol{A}^{R}\frac{1}{r}\ddot{M}_0\left(t - \frac{r}{\beta}\right) \tag{8}$$

with

$$\boldsymbol{A}^{R} = \cos\theta \sin\phi\hat{\boldsymbol{\theta}} + \cos 2\theta \cos\phi\hat{\boldsymbol{\phi}} \tag{9}$$

as the rotational radiation pattern (Cochard et al. 2006). Figure 9 shows the (a) translational and (b) rotational radiation patterns for a source in the XY-plane. Blue, red, and pink are the radiation patterns for the P-wave, S-wave, and rotation, respectively. The black, red, and blue circles mark positions of equally spaced stations in the XY-, XZ-, and YZ-plane around the source, respectively. It is easy to see that the biggest amplitude variations with azimuth are to be expect for stations along the black ring in the XY-plane, i.e. in plane with the source.

The Figs. 10 and 11 show the theoretical waveforms at the stations around the source shown in Fig. 9 in cartesian (ZXY) and spherical ($r\ \theta\ \phi$) coordinate systems,

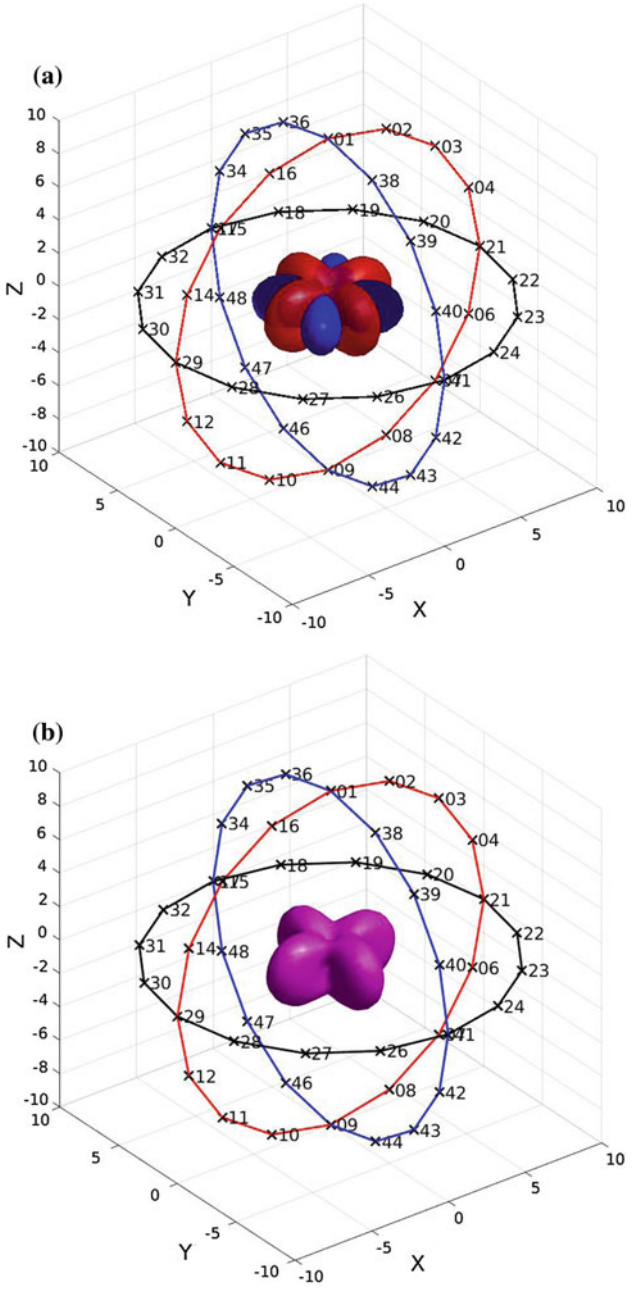

Fig. 9 Radiation patterns for slip in the XY-plane with slip in X direction in a homogeneous half-space. **a**, **b** are the radiation patterns for translational and rotational ground motions, respectively. In **a**, the blue and red radiation patterns are for P- and S-waves, respectively. Black, red, and blue circles mark positions of equally spaced stations in the XY-, XZ-, and YZ-plane, respectively. The colours and numbers correspond to the waveform colours and trace numbers in Figs. 10 and 11

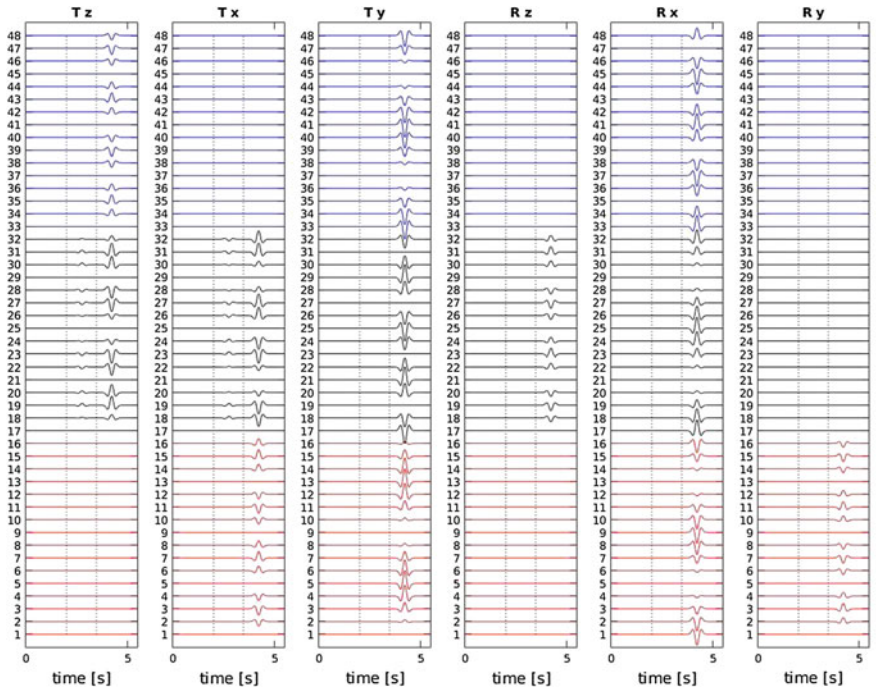

Fig. 10 Waveforms for the double-couple source of Fig. 9 in the ZXY coordinate system. Vertical numbers and waveform colours correspond to the three station rings around the source in Fig. 9. First three columns show translational displacement, while last three columns show rotational ground motions. Black dotted lines mark the time of the P-and S-wave arrivals. Waveforms are normalized preserving the ratios between the components. Rotational waveforms are additionally amplified by a factor 1.5×10^4

respectively. The colour-coding and numbering of the waveforms correspond to the station rings. As expected, the black waveforms for stations in-plane with the source show a clear signal on the majority of the traces compared to the waveforms of the other ring stations. The stations 17, 21, 25, and 29 are located on the nodal planes of the mechanism. In Fig. 11 there is only energy on their θ component, corresponding to the SH-wave energy of the source. The stations 19, 23, 27, and 31, rotated by 45° to the nodal planes, show the opposite behaviour with energy on the radial (P-wave energy) and the ϕ component (SV-wave energy) but no energy on the θ component.

Similar patterns can be found for the rotational waveforms. In the spherical coordinate system, the stations 21 and 29 have no rotation energy at all on all three components (nodal planes along rupture direction), while they show a maximum of rotation energy for the ϕ component at the stations 17 and 25 (nodal planes perpendicular to rupture direction). Slightly different, but still azimuth dependant energy patters are visible for the other two station rings.

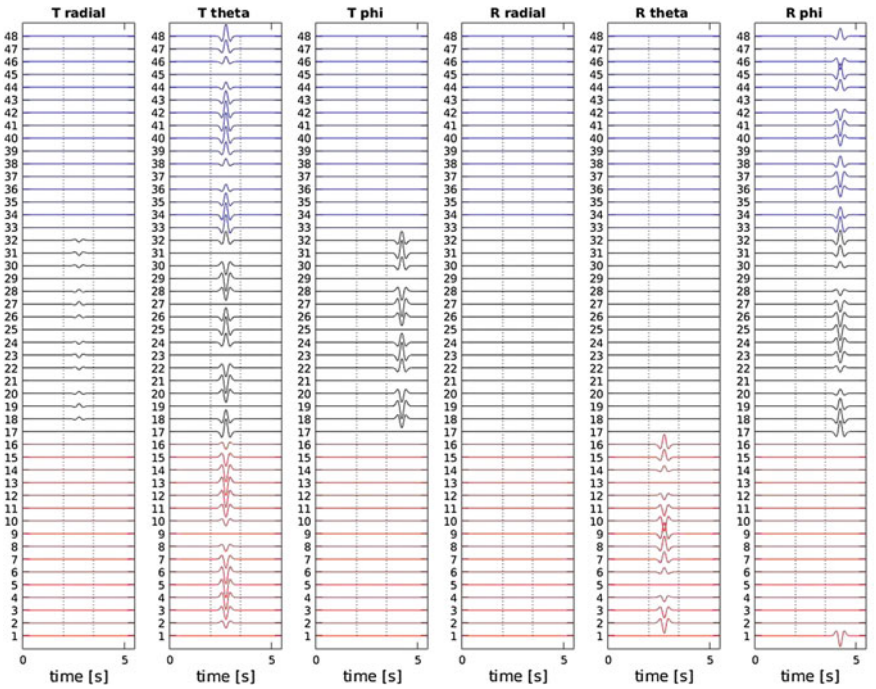

Fig. 11 Same as Fig. 10, the waveforms are now shown in the spherical coordinate system (r, θ, and ϕ) as used by e.g. Aki and Richards (2002)

These amplitude patterns in the form of ratios between the different components are the information needed to resolve the mechanism of an earthquake during inversion. When including rotational ground motion data to the inversion, 15 instead of only 3 amplitude ratios can be determined. Therefore, the position of the station within the radiation pattern can be much better constrained. As a consequence, the mechanism can be determined much more reliably, at least in cases of tectonic events where the double-couple part of the moment tensor should dominate.

References

Aki K, Richards PG (2002) Quantitative seismology, 2nd edn. University Science Book, Sausalito, CA

Banerdt WB, Smrekar S, Lognonné P, Spohn T, Asmar SW, Banfield D, Boschi L, Christensen U, Dehant V, Folkner W, Giardini D, Goetze W, Golombek M, Grott M, Hudson T, Johnson C, Kargl G, Kobayashi N, Maki J, Mimoun D, Mocquet A, Morgan P, Panning M, Pike WT, Tromp J, van Zoest T, Weber R, Wieczorek MA, Garcia R, Hurst K (2013) InSight: a discovery mission to explore the interior of Mars. In: Lunar and planetary science conference, vol 44 of Lunar and Planetary Inst. Technical Report

Bernauer M, Fichtner A, Igel H (2014) Reducing nonuniqueness in finite source inversion using rotational ground motions. J Geophys Res 119:4860–4875

Bernauer F, Wassermann J, Guattari F, Frenois A, Bigueur A, Gaillot A, de Toldi E, Ponceau D, Schreiber U, Igel H (2018) BlueSeis3A: full characterization of a 3C broadband rotational seismometer, SRL, https://doi.org/10.1785/0220170143

Beyreuther M, Barsch R, Krischer L, Megies T, Behr Y, Wassermann J (2010) ObsPy: a python toolbox for seismology. Seismol Res Lett 81:530–533

Bukchin B (2006) Specific features of surface wave radiation by shallow sources. Phys Solid Earth 42:712–717

Bukchin B, Clévédé E, Mostinskiy A (2010) Uncertainty of moment tensor determination from surface wave analysis for shallow earthquakes. J Seismol 14:601–614

Cochard A, Igel H, Schuberth B, Suryanto W, Velikoseltsev A, Schreiber U, Wassermann J, Scherbaum F, Vollmer D (2006) Rotational motions in seismology: theory, observation, simulation. In: Teisseyre R, Majewski E, Takeo M (eds) Earthquake source asymmetry. Structural Media and Rotation Effects, Springer, Berlin Heidelberg

Donner S, Rößler D, Krüger F, Ghods A, Strecker MR (2013) Segmented seismicity of the Mw 6.2 Baladeh earthquake sequence (Alborz mountains, Iran) revealed from regional moment tensors. J Seismol 17:925–959

Donner S, Bernauer M, Igel H (2016) Inversion for seismic moment tensors combining translational and rotational ground motions. Geophys J Int 207:562–570

Ekström G, Dziewonski AM, Steim JM (1986) Single station CMT: application to the Michoacan, Mexico, earthquake of September 19, 1985. Geophys Res Lett 13:173–176

Fan G, Wallace T (1991) The determination of source parameters for smaller earthquakes from a single, very broadband seismic station. Geophys Res Lett 18:1385–1388

Fichtner A, Kennett BLN, Igel H, Bunge H-P (2009) Spectral-element simulation and inversion of seismic waves in a spherical section of the Earth. J Numer Anal Ind Appl Math 4:11–22

Hastings WK (1970) Monte Carlo sampling methods using Markov chains and their applications. Biometrika 57:97–109

Jiménez E, Cara M, Rouland D (1989) Focal mechanisms of moderate-size earthquakes from teh analysis of single-station three-component surface wave records. Bull Seismol Soc Am 79:955–972

Krischer L, Megies T, Barsch R, Beyreuther M, Lecocq T, Caudron C, Wassermann J (2015) ObsPy: a bridge for seismology into the scientific Python ecosystem. Comput Sci Discov 8:014003

Megies T, Beyreuther M, Barsch R, Krischer L, Wassermann J (2011) ObsPy—What can it do for data centers and observatories. Ann Geophys 54:47–58

Metropolis N, Rosenbluth MN, Teller AH, Teller E (1953) Equation of state calculations by fast computing machines. J Chem Phys 21:1087–1092

ObsPy Development Team (2015). ObsPy 0.10.1. https://doi.org/10.5281/zenodo.16248

Reinwald M, Bernauer M, Igel H, Donner S (2016) Improved finite-source inversion through joint measurements of rotational and translational ground motions: a numerical study. Solid Earth 7:1467–1477

Tarantola A (2005) Inverse problem theory and methods for model parameter estimation, 2nd edn. Society for Industrial and Applied Mathematics, Philadelphia, Penn